THE JOURNAL OF BIOLOGICAL CHEMISTRY VOL. 285, NO. 32, pp. 24717–24728, August 6, 2010

Two Golgi-resident 3′-Phosphoadenosine 5′-Phosphosulfate Transporters Play Distinct Roles in Heparan Sulfate Modifications and Embryonic and Larval Development in *Caenorhabditis elegans*[*] [S]

Received for publication, November 26, 2009, and in revised form, April 23, 2010 Published, JBC Papers in Press, June 6, 2010, DOI 10.1074/jbc.M109.088229

Katsufumi Dejima[‡§1], Daisuke Murata[‡§], Souhei Mizuguchi[‡§2], Kazuko H. Nomura[‡§], Tomomi Izumikawa[§¶], Hiroshi Kitagawa[§¶], Keiko Gengyo-Ando[§‖3], Sawako Yoshina[§‖], Tomomi Ichimiya[**], Shoko Nishihara[**], Shohei Mitani[§‖], and Kazuya Nomura[‡§4]

From the [‡]Department of Biology, Faculty of Sciences 33, Kyushu University, Fukuoka 812-8581, Japan, the [§]Core Research for Evolutional Science and Technology (CREST), Japan Science and Technology Agency (JST), 4-1-8 Hon-cho, Kawaguchi, Saitama 332-0012, Japan, the [¶]Department of Biochemistry, Kobe Pharmaceutical University, Higashinada-ku, Kobe 658-8558, Japan, the [‖]Department of Physiology, Tokyo Women's Medical University School of Medicine, Tokyo 162-8666, Japan, and the [**]Laboratory of Cell Biology, Department of Bioinformatics, Faculty of Engineering, Soka University, 1-236 Tangi-cho, Hachioji, Tokyo 192-8577, Japan

Synthesis of extracellular sulfated molecules requires active 3′-phosphoadenosine 5′-phosphosulfate (PAPS). For sulfation to occur, PAPS must pass through the Golgi membrane, which is facilitated by Golgi-resident PAPS transporters. *Caenorhabditis elegans* PAPS transporters are encoded by two genes, *pst-1* and *pst-2*. Using the yeast heterologous expression system, we characterized PST-1 and PST-2 as PAPS transporters. We created deletion mutants to study the importance of PAPS transporter activity. The *pst-1* deletion mutant exhibited defects in cuticle formation, post-embryonic seam cell development, vulval morphogenesis, cell migration, and embryogenesis. The *pst-2* mutant exhibited a wild-type phenotype. The defects observed in the *pst-1* mutant could be rescued by transgenic expression of *pst-1* and *hPAPST1* but not *pst-2* or *hPAPST2*. Moreover, the phenotype of a *pst-1*;*pst-2* double mutant were similar to those of the *pst-1* single mutant, except that larval cuticle formation was more severely defected. Disaccharide analysis revealed that heparan sulfate from these mutants was undersulfated. Gene expression reporter analysis revealed that these PAPS transporters exhibited different tissue distributions and subcellular localizations. These data suggest that *pst-1* and *pst-2* play different physiological roles in heparan sulfate modification and development.

Organogenesis, tissue morphogenesis, and cell growth require diverse types of extracellular sulfation. Sulfated molecules are crucial for the establishment of a hydrophilic extracellular environment and for intercellular signaling (1–8). In eukaryotes, Golgi-resident sulfotransferases transfer sulfates from an active sulfate, 3′-phosphoadenosine 5′-phosphosulfate (PAPS),[5] to membrane-associated and secreted molecules like glycosaminoglycans (GAGs) (9–11). The sulfation reaction yields 3′-phosphoadenosine 5′-phosphate (PAP) as a byproduct. Biochemical and cytological studies have revealed that PAPS is synthesized by PAPS synthase, a bifunctional enzyme found in the nucleus and/or cytosol but not in the Golgi apparatus (12–15). PAPS transporters transport PAPS from the cytosol into the Golgi lumen (16). Recent reports have demonstrated that PAPS/PAP concentrations in the Golgi apparatus are important for biosynthetic regulation of sulfated molecules, including heparan sulfate (HS) (17–20). Thus, understanding how PAPS metabolism is regulated by PAPS transporters *in vivo* will provide important insight into the mechanisms underlying developmental control of extracellular sulfation.

PAPS transporter activity was first demonstrated in rat liver Golgi-derived vesicles (16). The characterization of purified proteins involved in PAPS transport activity suggests that they act through an antiport mechanism (13, 21–24). Recently, two human PAPS transporter genes were cloned and named *PAPST1* (*Slc35b2*) (25) and *PAPST2* (*Slc35b3*) (26, 27). The *Drosophila slalom* gene, which encodes PAPST1, was identified as a segment polarity gene (28, 29). In zebrafish, mutations in *pinscher*, the gene encoding PAPST1, caused defects in skeletal development and axon sorting (30). Although the gene encoding PAPST2 showed genetic interactions with the genes that

* This work was supported by a grant-in-aid from the Japan Society for the Promotion of Science Fellows (to K. D.), a grant-in-aid for young scientists (B) (to S. M.), and Grant-in-Aid for Scientific Research B-21390025 (to H. K.) from the Ministry of Education, Culture, Sports, Science, and Technology (MEXT), Japan. This research was also supported by MEXT Grant-in-Aid for Scientific Research B-20370051 (to S. N.) and by the Core Research for Evolutional Science and Technology Program of the Japan Science and Technology Corp. (to K. N.).

[S] The on-line version of this article (available at http://www.jbc.org) contains supplemental Figs. S1–S4 and Table S1.

[1] Present address: Dept. of Genetics, Cell Biology and Development, University of Minnesota, Minneapolis, MN 55455.

[2] Present address: Dept. of Tumor Genetics and Biology, Graduate School of Medical Sciences, Kumamoto University, Kumamoto, Japan.

[3] Present address: Saitama University Brain Science Institute, Saitama 338–8570, Japan.

[4] To whom correspondence should be addressed: Dept. of Biology, Faculty of Sciences, Kyushu University, Fukuoka 812-8581, Japan. Tel. and Fax: 81-92-642-4613; E-mail: knomuscb@kyushu-u.org.

[5] The abbreviations used are: PAPS, 3′-phosphoadenosine 5′-phosphosulfate; DIC, differential interference contrast; DTC, distal tip cell; EGFP, enhanced green fluorescent protein; GFP, green fluorescent protein; GAG, glycosaminoglycan; HA, hemagglutinin; hPAPST, human PAPS transporter; HS, heparan sulfate; PAP, 3′-phosphoadenosine 5′-phosphate; Sqv, squashed vulva; NS, 2-*N*-sulfate; 2*S*, 2-*O*-sulfate; 6*S*, 6-*O*-sulfate.

encode HS modification enzymes in the fruit fly, its physiological roles are largely unknown (27).

The nematode *Caenorhabditis elegans* is a model organism that is well suited for developmental genetics because of its simple and well organized organs, including those of the reproductive, digestive, nervous, and epithelial tissue systems. The *C. elegans* genome contains orthologs of all the known enzymes involved in PAPS metabolism, including PAPS synthase (*pps-1*, T14G10.1), PAPS reductase (R53.1), Golgi-resident PAP phosphatase (Y6B3B.5), sulfate transporters (*sulp-2*, F14D12.5; *sulp-4*, K12G11.1) (31), and PAPS transporters (*pst-1*, M03F8.2; *pst-2*, F54E7.1). In addition, *C. elegans* expresses genes that are involved in the sulfation of tyrosine and HS but not chondroitin (32–36). This represents an advantage of using *C. elegans* over vertebrate species to investigate the role of PAPS metabolism in development. In vertebrates, chondroitin sulfate is required for chondrogenesis (2, 18, 19, 30), and defects in chondroitin sulfation obscure the importance of other sulfated molecules. Previous studies have demonstrated that extracellular sulfated molecules play pivotal roles in nervous system development, gonadal cell migration, cuticle formation, and embryogenesis in *C. elegans* (37–42). Most recently, *pst-1* alleles were shown to be required for viability and neuronal development (43).

In this study, we aimed to investigate the roles of PAPS transporters in development and morphogenesis. To that end, we isolated *C. elegans* deletion mutants of the PAPS transporters and analyzed the defects in development and morphogenesis.

EXPERIMENTAL PROCEDURES

Materials—[^{35}S]PAPS (1.59 Ci/mmol), GDP-[U-^{14}C]fucose (271 mCi/mmol), and CMP-[9-^{3}H]sialic acid (33.6 Ci/mmol) were purchased from PerkinElmer Life Sciences. UDP-[6-^{3}H]galactose (20 Ci/mmol), UDP-*N*-acetyl-D-[6-^{3}H]galactosamine (20 Ci/mmol), UDP-[1-^{3}H]glucose (20 Ci/mmol), GDP-[2-^{3}H]mannose (40 Ci/mmol), UDP-[U-^{14}C]glucuronic acid (300 mCi/mmol), and UDP-[U-^{14}C]xylose (264 mCi/mmol) were purchased from American Radiolabeled Chemicals Inc. (St. Louis, MO). UDP-*N*-acetyl-D-[U-^{14}C]glucosamine (293 mCi/mmol) was purchased from GE Healthcare.

C. elegans Strains—We used *C. elegans* N2 as the wild-type strain. Strains were maintained and cultured as described previously (44). We used strains carrying the following alleles and balancer chromosomes: *ayIs4* I (45), *tm3316* III, *syIs80* III (46), *jcIs1* IV (47), *tm3364* V, and *nT1[qIs51]* (IV;V). All except *pst-1*(*tm3364*) and *pst-2*(*tm3316*) were obtained from the Caenorhabditis Genetic Center, which is funded by the National Institutes of Health, National Center for Research Resources (NCRR).

Isolation of Worms with Deleted Alleles—Worms with deletions of the *pst-1*(*tm3364*) and *pst-2*(*tm3316*) alleles were isolated from pools of worms that had been mutagenized by using the trimethylpsoralen/UV method (48). The *pst-1*(*tm3364*) mutant contained an 1186-bp deletion and a 9-bp insertion, which removed the third and fourth exons of the gene and resulted in a frameshift mutation. These deleted exons are identical among the three *pst-1* splice variants. The *pst-1*(*tm3364*) deletion mutant expressed only one transmembrane region in the N terminus of the protein. The *pst-2*(*tm3316*) mutant contained a 296-bp deletion that removed part of the fifth exon, resulting in a frameshift mutation. This deletion mutant expressed only five transmembrane regions in the N terminus of the protein. The *pst-1* deletion mutant was balanced and maintained as the *pst-1*(*tm3364*)/*nT1[qIs51]* strain. A double *pst-1;pst-2* deletion mutant was maintained as the *pst-1*(*tm3364*)/*nT1[qIs51]*, *pst-2*(*tm3316*) strain. To eliminate possible additional mutations, the *pst-1*(*tm3364*) and *pst-2*(*tm3316*) strains were back-crossed four and two times, respectively.

Analysis of GAGs—Freshly cultured nematodes were sonicated with a GE-70 ultrasonic processor (Branson Ultrasonics) and freeze-dried. The dried samples (136 mg of wild type, 72.8 mg of *pst-1*, and 182 mg of *pst-2*) were extracted with acetone and then treated with 6 ml of 1.0 M $NaBH_4$/0.05 M NaOH at 4 °C for 20 h. The reaction was stopped with the addition of acetic acid. The samples were adjusted to 5% trichloroacetic acid and centrifuged. The soluble fraction was extracted with ether. As shown previously (34, 49, 50), the amount of HS in *C. elegans* was extremely small; thus, for further processing, we added a carrier of 100 μg of shark cartilage chondroitin 6-*O*-sulfate (Seikagaku Corp.), which contained negligible amounts of non-sulfated disaccharides. The aqueous phase was adjusted to 80% ethanol. The resultant precipitate was dissolved in 50 mM pyridine acetate and subjected to gel filtration on a PD-10 column with 50 mM pyridine acetate as an eluent. The flow-through fraction was collected and evaporated. The dried samples were dissolved in water and applied to a column (7 ml) of cation-exchange resin AG 50W-X2 (H^+ form, Bio-Rad) pre-equilibrated with water. The unbound fraction, which contained the librated *O*-linked saccharides, was neutralized with 1 M NH_4HCO_3. The purified GAG fraction was digested with chondroitinase ABC or a mixture of heparitinases I and II, and then the digests were derivatized with 2-aminobenzamide and analyzed by high performance liquid chromatography as described previously (51).

Analysis of Embryonic Development—Four-dimensional microscopy was performed as described previously (49), except that embryos were mounted on a 2% agarose pad in M9 solution to examine the defects in the ventral cleft enclosure. This is because observation of the ventral cleft was difficult with embryos mounted on an 8-well printed microscopic glass slide (Matsunami Glass Inc.). To evaluate and compare the embryonic phenotypes of the mutants, embryos were dissected from the homozygous adult animals and cultured for 18 h in M9 at 20 °C.

Alkaline Bleach Assay—An alkaline bleach assay was performed basically as described (52). Ten adult hermaphrodites were transferred to a 5-μl M9 drop and placed on an 8-well glass slide followed by the addition of 2× alkaline hypochlorite solution (2 N NaOH, 80% NaOCl solution (10% available chlorine)). For the "time to stop thrashing," we recorded the time starting from the addition of hypochlorite and ending when all worms stopped thrashing.

Plasmid Construction—We generated plasmids that attached enhanced green fluorescent protein (*egfp*) or *mCherry* gene to the ends of different PAPS transporter or reporter genes. Plasmids were constructed on a pFX_EGFPT vector

backbone, essentially as described previously (53, 54), and named according to the gene they carried: $P_{pst\text{-}1a}$::*egfp*, $P_{pst\text{-}1bc}$::*egfp*, *pst-1ab(fl)*::*egfp*, *pst-1c(fl)*::*egfp*, $P_{pst\text{-}2}$::*egfp*, *pst-2a(fl)*::*egfp*, *pst-2b(fl)*::*egfp*, $P_{unc\text{-}119}$::*egfp*, and $P_{rgef\text{-}1}$::*egfp* ($P_{pst\text{-}1a}$ stands for *pst-1a* promoter and *fl* stands for full length (supplemental Figs. 1 and 2)). Briefly, cDNAs were amplified by reverse transcription-PCR from total RNA of wild-type *C. elegans* with specific primers tagged with the NotI restriction site. We inserted the cDNA fragments digested with NotI into the $P_{dpy\text{-}7}$::*egfp* or the $P_{dpy\text{-}7}$::*mCherry* plasmid to create $P_{dpy\text{-}7}$::*pst-1b*::*egfp*, $P_{dpy\text{-}7}$::*pst-2a*::*egfp*, and $P_{dpy\text{-}7}$::*aman-2*::*mCherry* (15, 55). Similarly, cDNAs were amplified by reverse transcription-PCR from total RNA of human prostate cancer (LNCaP) cells with specific primers tagged with NotI restriction sites, and cDNA fragments digested with NotI were cloned into the $P_{eft\text{-}4}$::*Venus* plasmid to make $P_{eft\text{-}4}$::*hPAPST1*::*Venus* and $P_{eft\text{-}4}$::*hPAPST2*::*Venus* (53). To make the tissue-specific *pst-1b*::*egfp* and *pst-2a*::*egfp* expression constructs, $P_{dpy\text{-}7}$::*pst-1a*::*egfp* and $P_{dpy\text{-}7}$::*pst-2a*::*egfp* were digested with NotI to yield the *pst-1a* and *pst-2a* sequences, respectively. These were cloned into $P_{myo\text{-}3}$::*egfp*, $P_{unc\text{-}119}$::*egfp*, and $P_{rgef\text{-}1}$::*egfp* plasmids. The plasmids for the yeast expression system were prepared using the GATEWAY™ cloning system (Invitrogen) as described previously (25–27). We used two steps of attB adaptor PCR for preparation of the attB-flanked PCR products. The first PCR step was performed with gene-specific primers, and the second PCR step was performed with attB adaptive primers. The PCR products of *pst-1a* and *pst-2* were cloned into pDONR™201. Then each construct was converted into a yeast expression vector, YEp352GAP-II, which was inserted into additional attB cassettes sequences and three influenza HA epitope tag sequences at the position of the multicloning site of YEp352GAP-II. YEp352GAP-II-*pst1a-HA* and YEp352GAP-II-*pst2-HA* plasmids were transformed into yeast. DNA sequence analysis was performed with the Prism 3130 Genetic Analyzer (Applied Biosystems). The PCR primers used in this section are listed in Table S1.

DNA Microinjection—Microinjections were performed as described by Mello and Fire (56). Expression constructs under the control of the *eft-4* promoter or other promoters were injected at 2–10 or 30 ng/μl, respectively, with co-injection of a tissue-specific marker, $P_{tph\text{-}1}$::*dsred* or $P_{aman\text{-}2}$::*aman-2*::*mCherry* at 20 ng/μl and/or *rol-6*(*gf*) at 80 ng/μl.

Subcellular Fractionation of Yeast and Transport Assay—Golgi-rich subcellular fractionation and nucleotide sugar transport assays were performed as described previously (25–27). Each YEp352GAP-II-*pst-1a-HA* and YEp352GAP-II-*pst-2-HA* plasmid was transformed into yeast (*Saccharomyces cerevisiae*) strain W303-1a (*MATa*, *ade2–1*, *ura3–1*, *his3–11,15*, *trp1–1*, *leu2–3,112*, and *can1–100*) by the lithium acetate procedure. These transformed yeast cells were grown at 30 °C in a synthetic defined medium lacking uracil. Yeast cells were converted into spheroplasts, homogenized, and fractionated to yield a 100,000 × *g* Golgi-rich subcellular fraction. Then, each Golgi-rich membrane fraction (200 or 100 μg of protein) was incubated in 50 μl of reaction buffer (20 mM Tris-HCl, pH 7.5, 0.25 M sucrose, 5.0 mM $MgCl_2$, 1.0 mM $MnCl_2$, and 10 mM 2-mercaptoethanol) that contained various substrates (mixture of radiolabeled and cold substrate) at 25 °C for 5 min. After incubation, the radioactivity incorporated in the Golgi-rich subcellular fractionation was trapped using a 0.45-μm nitrocellulose filter (Advantec MFS) and measured using liquid scintillation. The amount of radioactivity incorporated was calculated as the difference from the background value obtained from the same assay at 0 min for each sample.

Western Blot Analysis—The Golgi-rich subcellular fraction samples were suspended in 3× SDS sample buffer (New England Biolabs) and incubated 4 °C for 16 h. The samples were subjected to 10% SDS-polyacrylamide gel electrophoresis. The membrane to which the separated proteins were transferred was probed with anti-HA monoclonal antibody (Santa Cruz Biotechnology, Santa Cruz, CA) and horseradish peroxidase-conjugated anti-mouse IgG antibody and stained with ECL Plus (GE Healthcare).

Analysis of Subcellular Localization of PST-1·EGFP and PST-2·EGFP—To determine subcellular localization of the PST-1·EGFP protein, transgenic animals carrying extrachromosomal arrays of $P_{dpy\text{-}7}$::*pst-1b*::*egfp* and $P_{dpy\text{-}7}$::*aman-2*::*mCherry* were freeze-cracked and fixed in methanol for 5 min at −20 °C (57). After blocking with TBST (Tris-buffered saline containing 0.2% Tween 20), samples were incubated with the anti-GFP monoclonal antibody (1:100 dilution, mFX73; Wako Pure Chemical Industries) and anti-DsRed polyclonal antibody (1:100 dilution, Clontech) at room temperature for 2 h. Then, samples were washed twice with TBST and incubated at room temperature for 2 h with Alexa 488- or 594-conjugated anti-mouse IgG (H+L) (Molecular Probes) and/or Alexa 594-conjugated anti-rabbit IgG secondary antibody (Molecular Probes), diluted 1:200. Subcellular localization of the PST-2·EGFP protein was determined by examining transgenic animals that carried extrachromosomal arrays of *pst-2a(fl)*::*egfp* and $P_{aman\text{-}2}$::*aman-2*::*mCherry*. The specimens were observed on a Zeiss LSM510 system (Carl Zeiss). The extent of co-localization of PST-1·EGFP and PST-2·EGFP with AMAN-2·mCherry was determined as the percent intensity of the co-localized signal relative to the total GFP-specific signal using the colocalization threshold plug-in within NCBI Image J software.

RESULTS

Identification of C. elegans PAPS Transporter Genes pst-1 and pst-2—Only a single orthologous gene for each human PAPS transporter is found in the *C. elegans* genome: *pst-1* (M03F8.2) and *pst-2* (F54E7.1) (54, 33). The amino acid sequence of the human PAPS transporter-1 (hPAPST1) is 40.0, 40.5, and 36.3% identical to that of PST-1a, PST-1b, and PST-1c, respectively (supplemental Fig. S1*A*). On the other hand, the human PAPS transporter-2 (hPAPST2) amino acid sequence is 40.3 and 30.1% identical to that of PST-2a and PST-2b, respectively (supplemental Fig. S2*A*). The Web tool Phobius (58, 59) predicted that all the PST-1 variants possess nine transmembrane regions, whereas PST-2a and PST2b possess 10 and six transmembrane regions, respectively (supplemental Figs. S1*A* and S2*A*). The *C. elegans* genome database (Wormbase) indicates that the *pst-1* and *pst-2* loci encode three and two splice variants, respectively, and both loci are included in operons (OP5092 and OP3316) (supplemental Figs. S1*B* and S2*B*).

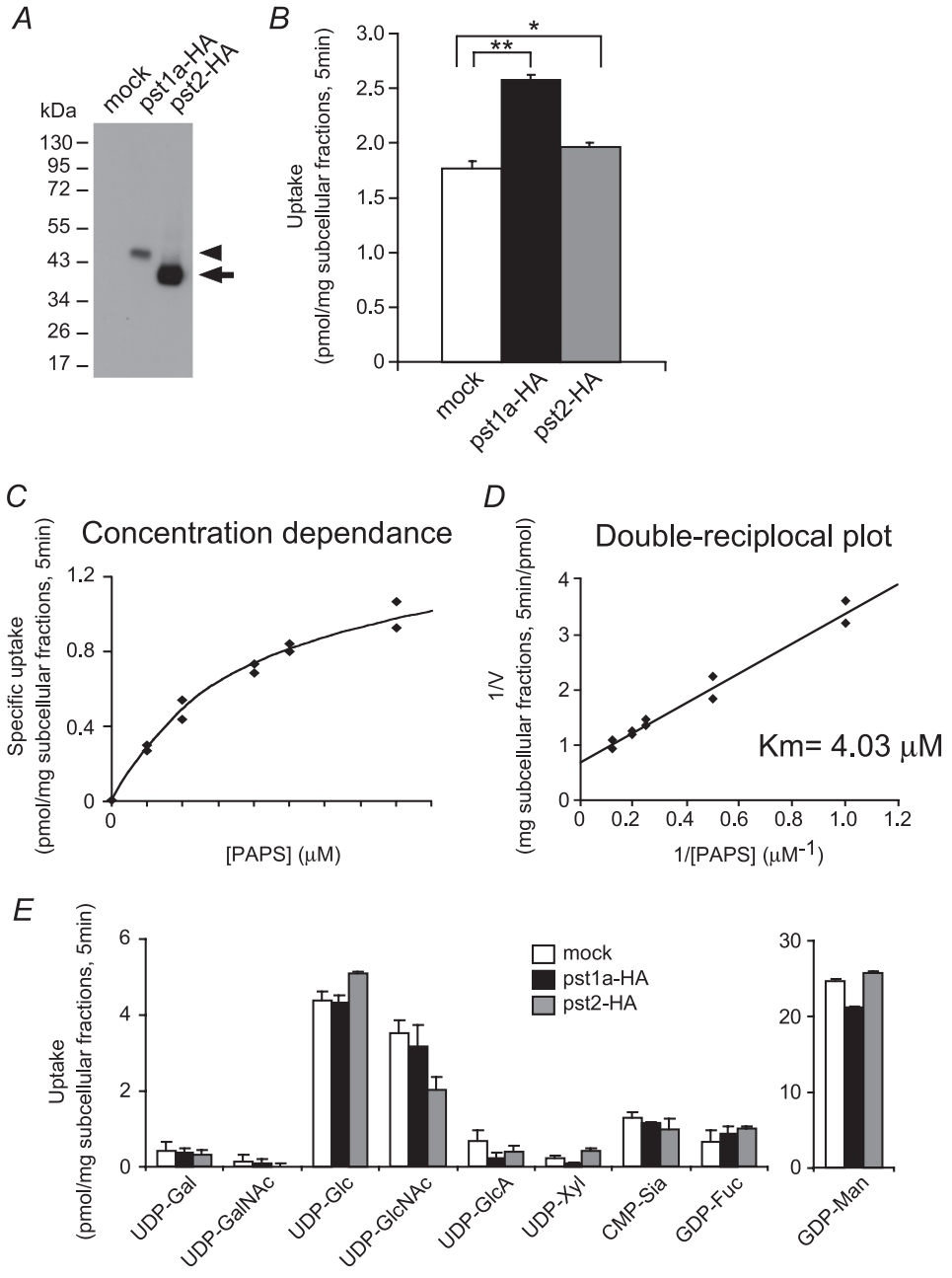

FIGURE 1. **Transport activities of PST-1a and PST-2 for PAPS and nucleotide sugars by yeast expression.** *A*, Western blot analysis of the Golgi-rich subcellular fraction prepared from yeast cells expressing mock (*left lane*), HA-tagged PST-1a (*center lane*), and HA-tagged PST-2 (*right lane*) using anti-HA monoclonal antibody. The loaded amount of subcellular fraction proteins was 5 μg from the cells expressing mock or HA-tagged PST-1a and 0.5 μg from the cells expressing HA-tagged PST-2. The *arrowhead* and *arrow* indicate HA-tagged PST-1a and HA-tagged PST-2, respectively. *B*, PAPS uptake of PST-1a and PST-2. 200 μg of Golgi-rich subcellular fraction for each sample was incubated in 50 μl of reaction buffer containing 5 μM PAPS (mixture of 2 μM [^{35}S]PAPS and 3 μM PAPS) at 25 °C for 5 min, and the incorporated radioactivity was measured. Values shown are the mean ± S.D. obtained from two independent experiments. *Open bar*, mock; *solid bar*, PST-1a-HA; *gray bar*, PST-2-HA. *, $p < 0.05$; **, $p < 0.001$; assessed by two-tailed Student's *t* test. *C*, substrate concentration dependence of PST-1a. 200 μg of Golgi-rich subcellular fraction for each sample was incubated in 50 μl of reaction buffer containing different concentrations of [^{35}S]PAPS at 25 °C for 5 min, and the incorporated radioactivity was measured. Specific uptake of PST-1a was calculated by subtracting the value of the mock uptake from the values of PST-1a-HA uptake. *D*, double-reciprocal plot used to determine the K_m value of PST-1a. *E*, nucleotide sugar uptake of PST-1a and PST-2. 100 μg of Golgi-rich subcellular fraction for each sample was incubated in 50 μl of reaction buffer containing 2 μM various nucleotide sugars at 25 °C for 5 min, and the incorporated radioactivity was measured. Values shown are the mean ± S.D. obtained from two independent experiments. *Open bar*, mock; *solid bar*, PST-1a-HA; *gray bar*, PST-2-HA.

Substrate Specificities of PST-1 and PST-2 Proteins Expressed in Yeast Cells—To determine the functional properties of PST-1 and PST-2, a heterologous yeast expression system was used (25–27). Western blot analysis demonstrated that PST-1a and PST-2 proteins were both expressed in the yeast P100 membrane fraction (Fig. 1*A*). The P100 fraction derived from yeast cells expressing PST-1a exhibited significant PAPS transport activity (Fig. 1*B*). The substrate concentration dependence on PAPS transport by PST-1a is shown in Fig. 1, *C* and *D*. The apparent K_m value of PST-1a was estimated to be 4.03 μM. PST-2 protein also exhibited statistically significant transport activity (Fig. 1*B*). However, the K_m value was not determined, because of its small transport activity. No significant difference was observed in transport activity of PST-1a and PST-2 for nucleotide sugars (Fig. 1*E*). These results suggest that the PST-1 and PST-2 proteins are PAPS-specific transporters.

Isolation of pst-1 and pst-2 Deletion Mutants—To gain insight into the physiological roles of PAPS transporters in *C. elegans*, we isolated strains with deletions in each of the *pst* genes from a library of trimethylpsoralen/UV-mutagenized worms by PCR screening. We isolated mutants that were predicted to have large transmembrane deletions in both alleles and thus likely to lack nucleotide sugar or PAPS transport activity (supplemental Figs. S1*A* and S2*A*). The isolated *pst-1*(*tm3364*) homozygotes had pleiotropic defects and an embryonic lethal phenotype (Fig. 2*B* and Table 1; also see below). In contrast, the isolated *pst-2*(*tm3316*) homozygotes were viable and fertile (Fig. 2*C* and Table 1; also see below) but had slightly reduced brood sizes (not shown).

Reduced HS Sulfation in pst-1(tm3364) and pst-2(tm3316) Mutant Worms—Next, we examined HS sulfation in the PAPS transporter mutants. Because of the embryonic lethality of the *pst-1*

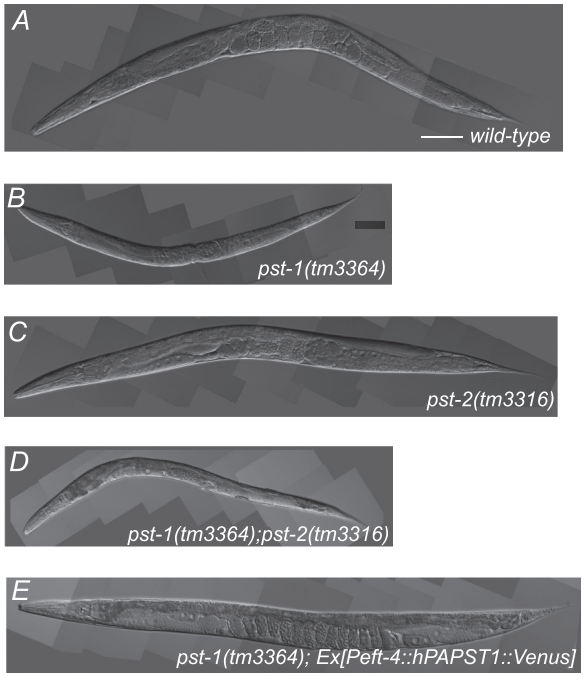

FIGURE 2. ***pst-1*(*tm3364*), *pst-2*(*tm3316*), and *pst-1*(*tm3364*);*pst-2*(*tm3316*) *C. elegans* mutants and transgenic rescue by hPAPST1.** *A–D*, representative DIC images of adult *C. elegans* wild type (*A*), *pst-1*(*tm3364*) mutant (*B*), *pst-2*(*tm3316*) mutant (*C*), and *pst-1*(*tm3364*);*pst-2*(*tm3316*) double mutant (*D*). The *pst-1*(*tm3364*);*pst-2*(*tm3316*) double mutant showed morphological features similar to those of the *pst-1*(*tm3364*) mutant. *E*, representative DIC image of an adult *pst-1*(*tm3364*) mutant expressing the *hPAPST1* transgene under the *eft-4* promoter ($P_{eft\text{-}4}$::*hPAPST1*::*Venus* construct). *Scale bar* = 100 μm.

TABLE 1

Summary of the phenotypes of PAPS transporter mutant animals

+, Abnormality was observed; ++, severe abnormality was observed; −, abnormality was not observed; ND, not determined.

Phenotype	*pst-1*(*tm3364*)	*pst-2*(*tm3316*)	*pst-1*, *pst-2*
Embryonic			
AB/P1 asymmetric cell division	−	−	ND
Cytokinesis	−	−	ND
EMS cell division	+	−	ND
Ea and Ep cell ingression	−	−	ND
Ventral enclosure	+	−	ND
Epidermal elongation	+	−	+
Larval			
Cuticle formation	+	−	++
Vulval morphology	+	−	+
Seam cell morphology	+	−	+
DTC migration	+	−	+

mutant, liquid culture samples containing *pst-1*(*tm3364*)/*nT1*[*qIs51*] heterozygous and *pst-1*(*tm3364*)/*pst-1*(*tm3364*) homozygous animals were used for biochemical analysis. For the *pst-2* mutant, liquid culture samples containing the *pst-2*(*tm3316*) homozygous animals were used. In wild-type worms, HS disaccharide analysis revealed the expected profile (Table 2) (15, 34, 35, 41). In both *pst-1* and *pst-2* mutant worms, the number of nonsulfated units increased, and the number of sulfated units decreased; this suggested that both *pst-1* and *pst-2* were involved in sulfation of HS *in vivo*. Notably, the disaccharide profile of the *pst-1* mutants was different from that of the *pst-2* mutant. The levels of trisulfated disaccharide units (ΔHexA(2*S*)α1–4GlcN(NS,6*S*)) were reduced in the *pst-1* mutant worms, but they were not affected in the *pst-2* mutant worms compared with the controls (N2 worms). Conversely, the levels of ΔHexAα1–4GlcNAc(6*S*) were not affected in the *pst-1* mutant worms, but they were reduced in the *pst-2* mutant worms compared with controls. These results suggest that sulfation patterns of HS depend on both PST-1 and PST-2 activity.

TABLE 2

Disaccharide composition of HS from *C. elegans* wild-type (N2) and mutant (*pst-1* and *pst-2*) strains

Disaccharide[a]	N2	*pst-1*[b]	*pst-2*[c]
		pmol/mg HS (%)	
ΔHexAα1–4GlcNAc[c]	23.6 ± 0.3 (47)	35.3 ± 0.8 (69)	22.6 ± 2.7 (71)
ΔHexAα1–4GlcNAc(6*S*)	4.8 ± 1.2 (10)	5.3 ± 3.0 (10)	1.5 ± 0.3 (5)
ΔHexAα1–4Glc(NS)	12.9 ± 1.7 (26)	8.2 ± 3.2 (17)	4.9 ± 2.3 (15)
ΔHexA(2*S*)α1–4Glc(NS)	7.2 ± 1.9 (14)	1.6 ± 0.5 (3)	1.7 ± 1.0 (5)
ΔHexA(2*S*)α1–4Glc(NS,6*S*)	1.6 ± 0.5 (3)	0.7 ± 0.1 (1)	1.0 ± 0.4 (3)
Total disaccharide	50.1 ± 3.5	51.1 ± 5.9	31.7 ± 3.6
Sulfation degree[d]	0.74	0.37	0.40

[a] ΔHexAα, Glc, and GlcNAc represent unsaturated hexuronic acid, glucosamine, and *N*-acetylglucosamine, respectively.
[b] Liquid culture samples containing *pst-1*(*tm3364*)/*nT1*[*qIs51*] heterozygotes and *pst-1*(*tm3364*)/*pst-1*(*tm3364*) homozygotes were used.
[c] Liquid culture samples containing only *pst-2*(*tm3316*) homozygous animals were used.
[d] Sulfation degree is expressed as the average number of sulfate groups/disaccharide unit.

Defects in pst-1 Are Rescued by Expression of Human PAPS Transporter-1 but Not Human PAPS Transporter-2—We performed rescue experiments in *pst-1* mutant worms by injecting plasmid constructs that carried wild-type genes under the *eft-4* promoter, which is active in almost all cells (41). Transgenic expression of *pst-1b*::*egfp* in *pst-1*(*tm3364*) animals rescued all the observed defects. This suggested that the *eft-4* promoter was sufficient to drive expression of constructs in cells that lacked PST-1 function (not shown). hPAPST1 and hPAPST2 are well characterized human Golgi-resident PAPS transporters (25, 26, 27). Transgenic expression of *hPAPST1*::*Venus* also rescued all of the defects observed in *pst-1*(*tm3364*) animals; this suggested that PST-1 is the homolog of the human PAPS transporter-1 (Fig. 2*E*). However, expression of *hPAPST2*::*Venus* did not rescue any of the defects, although we confirmed that the hPAPST2 protein was expressed in the transgenic worms (data not shown).

PST-1 Is Required for Cuticle Formation—Homozygous *pst-1*(*tm3364*) embryos from the *pst-1*(*tm3364*) heterozygous hermaphrodites hatched and developed into small, fragile L3 (5%), L4 (44%), or adult (51%) animals with impaired cuticles (n = 82; Fig. 2*B*). In contrast, development of *pst-2*(*tm3316*) homozygotes was similar to that of the wild type (Fig. 2*C*). Although *pst-1*(*tm3364*) mutant larvae exhibited apparently normal locomotion nematode growth medium agar plate during the L3 stage, they exhibited "skiddy" locomotion during the L4 to adult stages (not shown). A previous report showed that skiddy locomotion is correlated with a defect in cuticle formation (52). Differential interference contrast (DIC) microscopy analysis showed that the cuticle started to become irregular in the early L3 stage (compare Fig. 3, *A* and *C*). During the L4 to adult stages, the cuticle became more severely abnormal, resulting in defective molting with some blisters (compare Fig. 3, *B* and *D*). The old, unshed cuticle remained attached to the body in various places. In contrast, no cuticle abnormality was observed in the *pst-2*(*tm3316*) mutant worms. We also examined cuticle

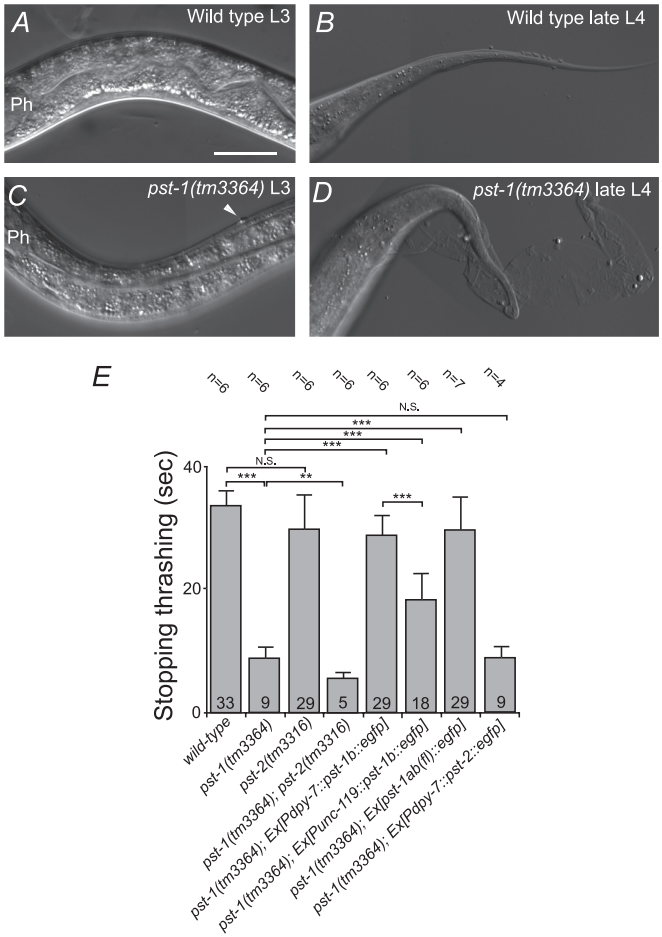

FIGURE 3. **Cuticle defect phenotype in *pst-1*(*tm3364*), *pst-2*(*tm3316*), and *pst-1*(*tm3364*);*pst-2*(*tm3316*) *C. elegans* mutant adult animals.** *A–D*, representative DIC images of regions behind the head (*A* and *C*) and tail (*B* and *D*) of wild-type L3 (*A*), wild-type late-L4 (*B*), *pst-1*(*tm3364*) mutant L3 (*C*), and *pst-1*(*tm3364*) mutant late-L4 larvae (*D*). *Ph*, posterior pharyngeal bulb; *arrowhead* (in *C*), in *pst-1*(*tm3364*) L3 larvae, some small protuberances of outer cuticle were observed, which were not observed in wild-type animals. During mid-L4 to the young adult stage, *pst-1*(*tm3364*) mutant animals showed abnormal molting (*D*). *Bar* = 30 μm. *E*, analysis of alkaline bleach sensitivity. The time to stop thrashing in alkaline bleach solution was an indicator of cuticle fragility. The *pst-1*(*tm3364*) mutant animals were more fragile (stopped faster) than the wild-type animals. In contrast, *pst-2*(*tm3316*) mutants showed cuticle fragility similar to wild-type animals. The *pst-1*(*tm3364*);*pst-2*(*tm3316*) double mutant animals were more fragile than the *pst-1*(*tm3364*) single mutant animals. In transgenic *pst-1*(*tm3364*) mutant animals that carried an extrachromosomal array of $P_{dpy\text{-}7}$::*pst-1b*::*egfp* or $P_{unc\text{-}119}$::*pst-1b*::*egfp*, the cuticle fragility was restored to the wild-type level, but the former was slightly more fragile than the latter. In transgenic *pst-1*(*tm3364*) mutant animals that carried an extrachromosomal array of $P_{dpy\text{-}7}$::*pst-2*::*egfp*, the cuticle fragility was similar to that of *pst-1*(*tm3364*) mutants without the transgene. *Ex*, extrachromosomal array; *N.S.* = not significant. **, $p < 0.01$; ***, $p < 0.001$; assessed by two-tailed Student's *t* test.

fragility by testing alkaline bleach sensitivity (52). Consistently, mutant *pst-1*(*tm3364*) worms exhibited very fragile cuticles (rapidly stopped moving in the alkaline solution), whereas mutant *pst-2*(*tm3316*) worm cuticle fragility was similar to that of the wild-type animals (Fig. 3*E*).

PST-1 Is Required for Vulval Morphogenesis—DIC analysis showed that almost all *pst-1* knock-out animals exhibited various forms of disorganized vulval morphology. In 79% ($n = 39$) of *pst-1*(*tm3364*) mutant mid-L4 larvae, the vulva contained some abnormally positioned cells, which resulted in a longer invagination along the anterior-posterior axis or a small, ectopic invagination (Fig. 4, *A* and *B*). In 16% ($n = 8$) of *pst-1*(*tm3364*) mid-L4 larvae, vulval cells were arranged relatively normally but exhibited a collapsed invaginated space (Fig. 4*A*, *middle*) similar to that observed in the squashed vulva (Sqv) phenotype caused by a deficiency in chondroitin glycosaminoglycan synthesis (44, 49, 60, 61). The vulval architecture in the *pst-1*(*tm3364*) mutant was visualized with the transgenic expression of *ajm-1*::*gfp*, an adherence junction marker of epithelial and vulval cells. This showed a disturbance during the mid-L4 stage (Pn.pxxx stage) (Fig. 4*C*). A large fraction (43%) of the *pst-1*(*tm3364*) mutant animals exhibited a fragmented vulva, and 17.4% ($n = 23$) exhibited incorrectly positioned cells. This observation suggested that vulval cell migration and orientation are affected in *pst-1*(*tm3364*) mutants. A LIM class homeobox gene, *lin-11*, which is involved in specific cell fates of vulva cell types, was transgenically expressed with the $P_{lin\text{-}11}$::*gfp* construct. In wild-type secondary cells, *lin-11* typically shows an asymmetric expression pattern (46) (Fig. 4*D*). In *pst-1*(*tm3364*) mutants, the asymmetric *lin-11*::*gfp*(*syIs80*) expression pattern was irregular (Fig. 4*E*, 33.3%, $n = 15$) at the L3 stage (Pn.pxx stage), and expression levels were drastically reduced at the mid-L4 stage (Pn.pxxx stage) (Fig. 4*F*, 100%, $n = 20$). However, in VC motor neurons, *lin-11*::*gfp* expression was undisturbed (Fig. 4*D*).

Additionally, the expression levels of GFP were not affected in worms expressing $P_{egl\text{-}17}$::*gfp* where *egl-17* encodes a fibroblast growth factor family member, which is specifically expressed in secondary cells at the Pn.pxxx stage. However, the patterning of cells that expressed $P_{egl\text{-}17}$::*gfp* was affected at this stage (data not shown). These results suggested that secondary cell fate is adopted in *pst-1*(*tm3364*) and that PST-1 is involved in vulval morphogenetic events via regulation of *lin-11* expression.

PST-1 Is Required for Post-embryonic Seam Cell Development and Distal Tip Cell (DTC) Migration—Disruption of the *pst-1* gene resulted in abnormal seam cell development (see supplemental Fig. S3 and the legend for details). The results suggested that *pst-1* is involved in post-embryonic seam cell development. In addition to epithelial defects, *pst-1* mutant animals were also defective in DTC migration. During the L4 stage in most wild-type animals, two DTCs that reached the dorsal side migrated along the dorsal body wall muscles toward the middle of the animal (supplemental Fig. S3*E*). In *pst-1*(*tm3364*) mutant larvae, 26.4% ($n = 49$) of anterior and 45.6% ($n = 48$) of posterior DTCs failed to migrate along the dorsal side and remained on the ventral side in the early to mid-L4 stage (supplemental Fig. S3, *F* and *G*). In *pst-2*(*tm3316*) mutant larvae, no abnormalities in seam cell development or DTC migration were observed (supplemental Fig. S3*G*).

PST-1 Is Required during Embryogenesis for Oriented EMS Cell Division, Neuroblast Migration, and Epidermal Elongation—The second generation (F1) of *pst-1*(*tm3364*) homozygous embryos, which is predicted to lack both maternal and zygotic *pst-1* activity, displayed a fully penetrant embryonic lethal phenotype (Fig. 5*A*). This suggested that the first generation of *pst-1*(*tm3364*) homozygous embryos grew to adults because maternally supplied molecules rescued the deficient embryos. Two-thirds (67%) of the *pst-1*(*tm3364*) F1 embryos displayed

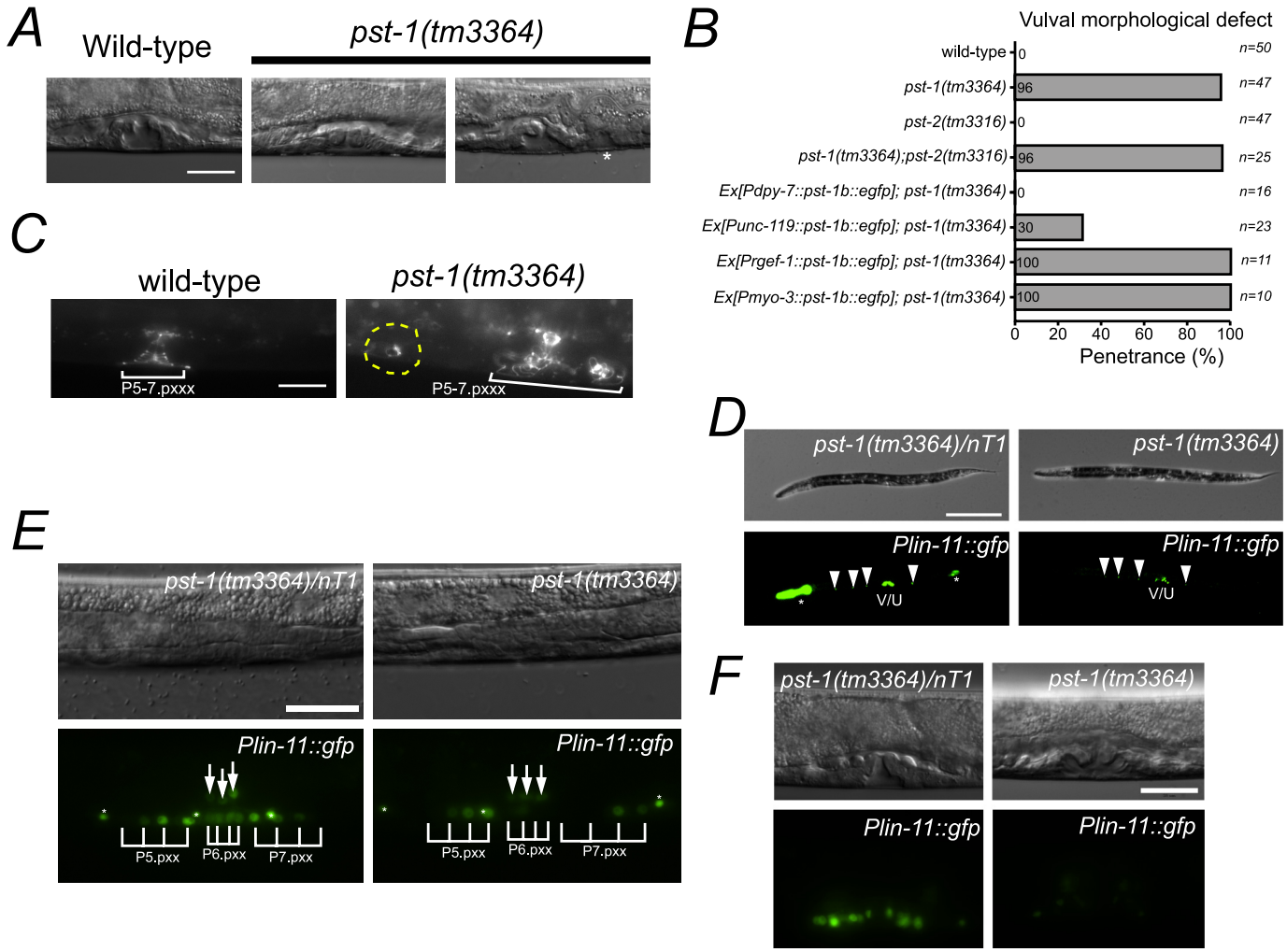

FIGURE 4. **Vulval defects of the *pst-1*(*tm3364*) mutant.** *A*, wild-type vulva forms an invagination space that looks like a pointed hat during early to mid-L4 stage (*left*). The *pst-1*(*tm3364*) mutation induced a collapse of the vulval invagination space (*middle*). In the mid-L4 stage, the *pst-1*(*tm3364*) vulva exhibited an ectopic invagination space (*asterisk*, *right panel*). *Scale bar* = 20 μm. *B*, penetrance in several genetic backgrounds of vulval morphological defects, including the squashed vulva and inappropriate vulval cell positioning. *Ex*, extrachomosomal array. *C*, the vulval structures of wild-type (*left*) and *pst-1*(*tm3364*) homozygote (*right*) animals were visualized with AJM-1·GFP. Incorrectly positioned cells are circled with a *yellow dashed line*. *Scale bar* = 20 μm. *D*, DIC and fluorescence images of *pst-1*(*tm3364*)/*nT1* (*left*) and *pst-1*(*tm3364*) homozygote (*right*) mid-L4 animals that expressed P_{lin-11}::*gfp*. The *pst-1*(*tm3364*)/*nT1* animals with the *syIs80* transgene showed P_{lin-11}::*gfp* expression patterns similar to those of wild-type animals (data not shown). The GFP signals derived from the *nT1[qIs51]* balancer chromosome are indicated with *asterisks*. *Arrowheads* indicate VC motor neurons, and *V/U* indicates P_{lin-11}::*gfp* expression in the vulva and uterus. *Bar* = 200 μm. *E*, DIC and fluorescence images of *pst-1*(*tm3364*)/*nT1* (*left*) and *pst-1*(*tm3364*) homozygote (*right*) vulvas during the L3 stage (Pn.pxx stage). GFP signals from VC motor neurons are indicated with *asterisks*. GFP signals from the uterus are indicated with *arrows*. *Bar* = 25 μm. *F*, DIC and fluorescence images of *pst-1*(*tm3364*)/*nT1* (*left*) and *pst-1*(*tm3364*) (*right*) homozygote vulvas during the mid-L4 stage (Pn.pxxx stage). *Bar* = 25 μm.

severe morphogenetic defects that resulted in disorganized morphology before the early stage of elongation; the other one-third (33%) displayed relatively mild morphogenetic defects that resulted in developmental arrest during the elongation stage. This embryonic phenotype was reminiscent of the disruption of HS synthesis by *rib-1* and *rib-2* knock-outs (40, 41, 62) or the disruption of PAPS synthesis (15). This supports the notion that *pst-1* is involved in HS sulfation during embryonic development. In contrast, embryos that lacked *pst-2* activity displayed little or no overt embryonic lethality (Fig. 5*A*). Analysis of *pst-1*(*tm3364*) F1 embryos by DIC optics revealed that none (n = 23) were affected in the initial step of gastrulation (ingression of Ea and Ep cells), but a small fraction of them were affected in EMS cell division orientation (6.9%, n = 29; Fig. 5, *B* and *C*). In wild-type embryonic morphogenesis, ventral neuroblasts migrated toward the ventral cleft created by the ingression of mesodermal cells, where they formed a substrate for the epidermis during ventral enclosure (63). In *pst-1*(*tm3364*) F1 embryos that exhibited severe morphogenetic defects, ventral enclosure failed, resulting in an unenclosed ventral surface (Fig. 5, *D* and *F*), suggesting that PST-1 was involved in neuroblast migration in the early morphogenesis phase. The *pst-1*(*tm3364*) F1 embryos that underwent normal ventral enclosure elongated to variable lengths ranging from 1.5- to 3-fold increases in size and then retracted, resulting in a swollen body morphology (Fig. 5, *E* and *G*).

Differential Expression Patterns of pst-1 and pst-2—To determine the localization of *pst-1* and *pst-2*, we injected four types of *pst-1* and three types of *pst-2* transgene expression vectors into wild-type animals. (Constructs and expression patterns summarized in supplemental Figs. S1*C* and S2*C* and Table 3.) In animals that carried the *pst-1ab(fl)*::*egfp*, *pst-1c(fl)*::*egfp*, and

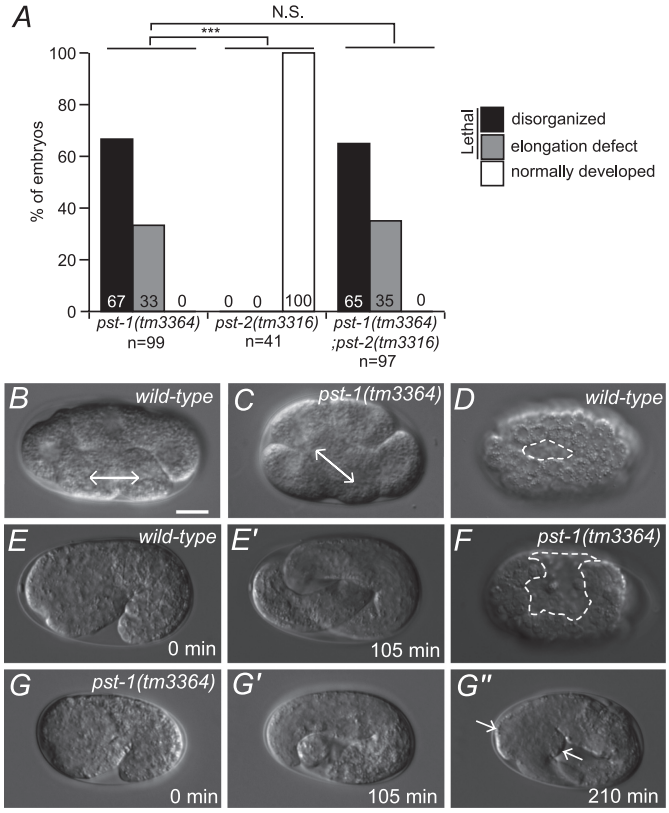

FIGURE 5. **Embryonic phenotypes of *pst-1* and *pst-2*.** *A*, percentage of embryonic mutant phenotypes in *pst-1*(*tm3364*), *pst-2*(*tm3316*), and double *pst-1*(*tm3364*);*pst-2*(*tm3316*) mutants. *N.S.*, not significant. ***, $p < 0.001$. *B* and *C*, EMS cell division axis is affected in *pst-1(tm3364)* embryos. In wild-type embryos at the 6-cell stage, EMS cells divide along the anterior/posterior axis (*bidirectional arrow* (*B*)). In *pst-1*(*tm3364*) mutant embryos at the 6-cell stage, the axis of EMS division is skewed (*bidirectional arrow* (*C*)). *D* and *F*, DIC images of wild-type (*D*) and *pst-1*(*tm3364*) (*F*) embryos at the ventral cleft enclosure stage. The *dashed lines* indicate the edges of an unenclosed ventral surface. *E–G″*, time lapse analysis of wild-type (*E* and *E′*) and *pst-1*(*tm3364*) (*G* and *G″*) embryos during the elongation stage. *Arrows* indicate swollen body morphology. *Scale bar* = 10 μm.

TABLE 3
Summary of the expression patterns of PAPS transporter genes

Reporter construct	Expression pattern
$P_{pst\text{-}1a}$::*egfp*	Ubiquitous
$P_{pst\text{-}1bc}$::*egfp*	Epidermis (amphid sheath cells, hypodermis, seam cells)
pst-1-ab(fl)::*egfp*	Epidermis (amphid sheath cells, hypodermis, seam cells)
pst-1c(fl)::*egfp*	Epidermis (amphid sheath cells, hypodermis, seam cells)
$P_{pst\text{-}2}$::*egfp*	Intestine, gland cells
pst-2a(fl)::*egfp*	Intestine, gland cells
pst-2b(fl)::*egfp*	No expression

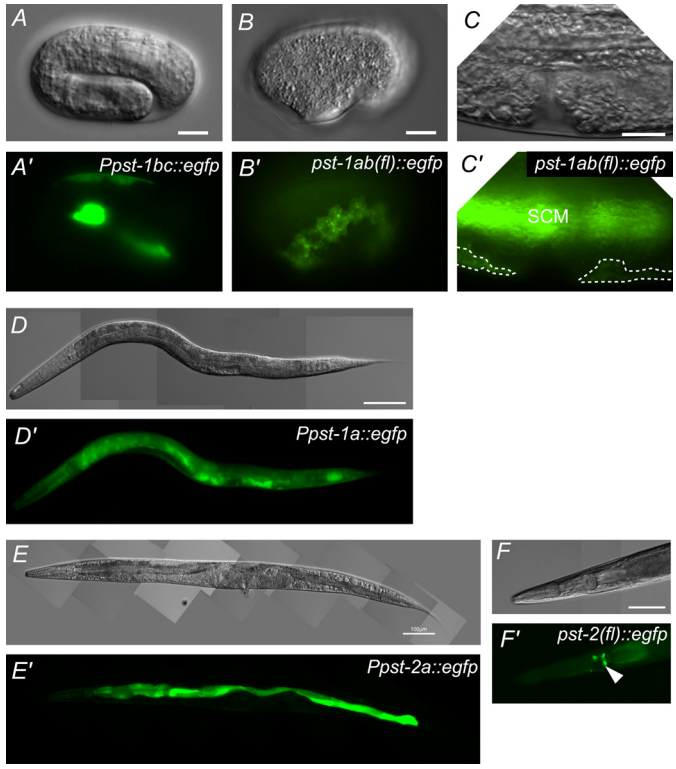

FIGURE 6. **Expression patterns of *pst-1* and *pst-2* reporter constructs in wild-type animals.** Transgene reporter analyses of *pst-1* (*A–D*) and *pst-2* (*E* and *F*). DIC (*A–F*) and fluorescent (*A′–F′*) images are shown. GFP was visualized directly under a fluorescence microscope except in *B′* and *C′*, which were sliced samples immunostained with an anti-GFP antibody. *A* and *A′*, expression pattern of $P_{pst\text{-}1bc}$::*egfp* in a folded embryo. EGFP is dominantly expressed in seam cells. *B*, *B′*, *C*, and *C′*, expression pattern of *pst-1ab(fl)*::*egfp* in an embryo (*B*) and the mid-ventral region (*C*) of a mid-L4 hermaphrodite. EGFP is dominantly expressed in seam cells. EGFP is expressed in seam cells (*SCM*) and the hypodermis (indicated with *dashed lines*) but not in the vulva (*C′*). *D* and *D′*, expression pattern of $P_{pst\text{-}1a}$::*egfp* in a mid-L4 larva. EGFP is expressed in almost all cells. *E* and *E′*, expression pattern of $P_{pst\text{-}2a}$::*egfp* in a young adult animal. EGFP is expressed in the intestine and pharyngeal gland cells. GFP expression in pharyngeal gland cells is weaker than in the intestine in this animal. *F* and *F′*, expression pattern of *pst-2(fl)*::*egfp* in the head region of a young adult animal. The EGFP signal in the pharyngeal gland cells is indicated with an *arrowhead*. *Scale bars* = 10 μm (*A–C*) and 100 μm (*E–F*).

$P_{pst\text{-}1bc}$::*egfp* vectors, GFP fluorescence was specifically observed in seam cells and amphid sheath cells during embryonic and larval development (Fig. 6, *A* and *B*). GFP expression was also detected in the hypodermis of L4 transgenic animals that carried *pst-1ab(fl)*::*egfp* (Fig. 6*C*) and *pst-1c(fl)*::*egfp*. Although the *pst-1* mutant displayed a vulval defect, no vulval expression was observed in these transgenic worms (Fig. 6*C*). In contrast, in transgenic animals that carried $P_{pst\text{-}1a}$::*egfp*, GFP fluorescence was observed in almost all cells throughout development except germ cells, where extrachromosomal transgenes are generally silenced (Fig. 6*D*). The *pst-1ab(fl)*::*egfp* and *pst-1c(fl)*::*egfp* constructs included the entire sequence of *pst-1a*, but $P_{pst\text{-}1a}$::*egfp* carried only the 5′-promoter region of *pst-1a*. Thus, broad expression of $P_{pst\text{-}1a}$::*egfp* might be induced due to the absence of a regulatory region for transgene expression. Additionally, the expression pattern induced by a promoter of the M03F8.3 gene, a gene immediately upstream of *pst-1*, was similar to that induced by the *pst-1a* promoter (sEx10297 transgene). Expression data from a genome-wide *in situ* hybridization analysis indicated that *pst-1* mRNA was specifically expressed in lateral seam cells, the adult germ line, and early embryos (a cDNA group, CELK04198, NextDB (nematode expression pattern database)).

In transgenic animals that carried the $P_{pst\text{-}2a}$::*egfp* and *pst-2(fl)*::*egfp* constructs, EGFP fluorescence was specifically observed in intestinal and pharyngeal gland cells (Fig. 6, *E* and *F*). However, no GFP signal was observed in worms carrying $P_{pst\text{-}2b}$::*egfp* (data not shown). This suggested that the *pst-2b*

promoter does not have inherent activity. Although there are no expression data for *pst-2* in the NextDB, *pst-2* is among the set of 603 germ line-specific/enriched genes identified by SAGE (serial analysis of gene expression). In the SAGE library, we found 10 tags for *pst-2* in the germ line and four tags in the soma, suggesting that *pst-2* is expressed predominantly in the germ line (64). Taken together, these results suggest that although both *pst-1* and *pst-2* are likely to be expressed in the germ line, they have mutually exclusive expression patterns in somatic cells; *pst-1* tends to be dominantly expressed in tissues generated from ectodermal cells, and *pst-2* tends to be expressed in tissues generated from endomesodermal cells.

PST-1 and PST-2 Are Localized to the Golgi Apparatus—In cultured mammalian cells, PAPS transporters have been shown to localize to the Golgi membrane (20, 25, 26). Our reporter analyses indicated that *pst-1* and *pst-2* are expressed in the hypodermis and intestine, respectively. Thus, we examined the subcellular localizations of PST-1·EGFP and PST-2·EGFP in those tissues. Consistent with the previous reports, the transporter proteins PST-1·EGFP and PST-2·EGFP co-localized with a marker of the Golgi apparatus, mCherry-tagged alpha-mannosidase II (AMAN-2). This suggested that PST-1 and PST-2 proteins reside in the Golgi (supplemental Fig. S4, *A* and *B*). However, in merged images, it was apparent that although PST-2·EGFP almost completely co-localized with AMAN-2, PST-1·EGFP only partly co-localized with AMAN-2 (supplemental Fig. S4*C*). The localization of AMAN-2 is predicted to be in the cis/medial-Golgi compartments rather than the trans-Golgi compartment. Thus, our results suggested that PST-2, but not PST-1, was distributed primarily in the cis/medial-Golgi compartments.

PST-1 Expression in the Epidermis Is Sufficient for Proper Larval Epithelial Development, and Its Expression in the Neuroectoblast Is Sufficient for Rescuing Embryonic Lethality—To determine which cell types required *pst-1* gene function, we examined whether epidermal, neuronal, or muscle expression of *pst-1* was sufficient to rescue the embryonic, vulval, and cuticle phenotypes of deletion mutants. Epidermis-specific expression of *pst-1b*::*egfp* under the control of the *dpy-7* promoter rescued vulval and abnormal cuticle phenotypes (Figs. 3*E* and 4*B*) and exhibited weak activity, but it was sufficient to rescue the embryonic phenotype (Table 4). The neuroectoderm- and neuron-specific expression of *pst-1b*::*egfp* under the control of the *unc-119* promoter only partially rescued vulval and abnormal cuticle phenotypes (Figs. 3*E* and 4*B*). However, it rescued the embryonic lethal phenotype more completely than epidermis-specific expression (Table 4). In contrast, differentiated neuron-specific or body wall muscle-specific expression of *pst-1b*::*egfp* under the control of *rgef-1* or *myo-3* promoters did not rescue any of the phenotypes. These results suggested that *pst-1* has specific functions in epidermal tissues during larval development and in epidermal precursors and/or neuroblasts during embryogenesis.

pst-2 Synergizes with pst-1 in Cuticle Formation but Not in Vulval Development or Embryogenesis—To investigate the genetic relationship between *pst-1* and *pst-2*, we examined the *pst-1*;*pst-2* double mutant phenotypes. The *pst-1* mutants exhibited abnormalities in embryogenesis, vulval development, and cuticle formation, but the *pst-2* mutants displayed essentially normal phenotypes (Figs. 3*E* and 4*B*). These data suggested that *pst-1* and *pst-2* do not have redundant roles in embryogenesis and vulval development. In contrast, the alkaline bleach sensitivity test revealed that the *pst-1*;*pst-2* double mutant had a more severely fragile cuticle than the *pst-1* single mutant (Fig. 3*E*), despite their similarities in DIC analyses. This suggested that *pst-1* and *pst-2* had some redundant functions in cuticle formation. To determine whether the redundancy between *pst-1* and *pst-2* resulted from the molecular function of the PAPS transporter, we ectopically expressed *pst-2* in the epidermis of the *pst-1*(*tm3364*) mutant and examined the effect on cuticle abnormality. The alkaline bleach sensitivity test revealed that *pst-2* expressed in the epidermis under control of the *dpy-7* promoter failed to rescue cuticle fragility in *pst-1*(*tm3364*) mutants; in contrast, *pst-1b* expression successfully rescued cuticle fragility (Fig. 3*E*). These results suggested that PST-1 and PST-2 play differential physiological roles in cuticle formation.

TABLE 4
Either neuroectodermal or epidermal expression of PST-1 was necessary and sufficient for embryogenesis

Promoter	Target tissue	No. of plates with proliferating progeny/ total test plates[a]	Rescue activity[b]
		10 larvae/plate	
None		0/2	−
pst-1bc	Hypodermis, seam cells, amphid sheath	2/2, 2/2[c]	++
dpy-7	Hypodermis, seam cells	3/5, 3/3[c]	+
unc-119	Neuroectoderm, differentiated neurons	2/2, 2/2[c]	++
rgef-1	Differentiated neurons	0/3	−
myo-3	Body wall muscles	0/3	−

[a] Ten L4 larvae of mutant or transgenic animals were transferred to a fresh plate seeded with OP50 to determine whether the animals could proliferate after 1 week.
[b] Lethality in transgenic *pst-1*(*tm3364*) mutant embryos that carried P_{dpy-7}::*pst-1b*::*egfp* was higher than in those that carried $P_{unc-119}$::*pst-1b*::*egfp* or *pst-1bc*(*fl*)::*egfp*.
[c] Two independent transgenic lines were tested.

DISCUSSION

This study showed that, in *C. elegans*, the PAPS transporter *pst-1* gene, but not the *pst-2* gene, is essential for diverse aspects of epithelial development, somatic gonadal cell migration, and viability. We observed embryonic defects in *pst-1* knock-out worms similar to those observed in embryos deficient in *pps-1* (15) or *rib-1/rib-2*, which lacked HS-synthesizing enzymes (41, 62). During larval development, the *pst-1* mutant showed defective cuticle formation similar to that observed in larvae depleted of *pps-1* or tyrosylprotein sulfotransferase-A (*tpst-1*) genes (15, 37). Although disaccharide analysis revealed that both *pst-1* and *pst-2* were involved in HS sulfation, none of the defects caused by the *pst-1* mutation could be restored by the heterogeneous expression of hPAPST2 or PST-2. Moreover, HS sulfation patterns isolated from *pst-1* mutant animals were clearly different from those isolated from *pst-2* mutant animals. Furthermore, *pst-1* and *pst-2* displayed different expression patterns. These observations indicated that hPAPST1/PST-1 has distinct characteristics from hPAPST2/PST-2 *in vivo*. Our data also suggested that subcellular localization of the PST-

1·EGFP protein was slightly different from that of the PST-2·EGFP protein. Thus, each PAPS transporter may reside in different intracellular compartments; this would allow differential sulfation reactions within a single cell. Intriguingly, differential "Golgi units" are proposed to regulate different glycosylation reactions in *Drosophila* cells (65).

Analysis using the yeast heterologous system clearly suggested that PST-1 and PST-2 are PAPS-specific transporters. Although PST-2 showed weaker transport activity compared with PST-1, the transporter activity in our assay was statistically significant, and PST-2 showed no transport activity for nucleotide sugars. These results together with the reduced sulfation in the *pst-2* null allele HS disaccharide analysis strongly indicate that PST-2 is also a PAPS transporter. It is intriguing that the total amount of HS disaccharide units was decreased in *pst-2* mutant but not in the *pst-1* null allele. Because sulfation takes place simultaneously with elongation of the GAG chain (66), depletion of PAPS in the intracellular compartment containing PST-2 may specifically influence the synthesis of GAG chains and reduce the heparan sulfate content measured in *pst-2* null mutant animals.

The *pst-1*, *pst-2* double mutant showed that PST-1 and PST-2 had synergistic effects in cuticle formation. Precise cuticle formation requires both epithelial cells and pharyngeal gland cells (67). Epithelial cells synthesize the cuticle, and pharyngeal gland cells are thought to secrete a surface coating that covers the cuticle. Our results showed that *pst-2* was expressed in pharyngeal gland cells, and thus in these cells, PST-2 may be involved in the secretion or synthesis of components of the cuticle surface coat. Another nucleotide sugar transporter, SRF-3, transports UDP-GlcNAc and UDP-Gal into Golgi apparatus-enriched vesicles from the cytosol. SRF-3 is expressed in pharyngeal gland cells and seam cells. It is involved in the biosynthesis of glycoconjugates for the outer surface and the cuticle (68, 69). Considering the expression patterns of PST-2, it is possible that PST-2 may cooperate with SRF-3 in this process. We also found that PST-2 was strongly expressed in the intestine, consistent with the tissue distribution of hPAPST2 transcripts (26). This implies that PST-2 and hPAPST2 may play a common role in the intestine; for example, they may participate in host-pathogen interactions.

Vulval morphogenesis, including invagination and final cell positioning along the anterior-posterior axis, was affected in *pst-1* mutant animals. Our data suggest that *pst-1* is required for the precise expression of *lin-11*::*gfp*. Similar findings have been reported for worms that expressed mutant *lin-17*, a gene that encodes the Frizzled Wnt receptor (46, 70, 71). HS proteoglycans are essential for Wnt signaling, both in vertebrates and invertebrates (72), and thus the sulfation of HS proteoglycans could modulate Wnt/Frizzled signaling or *lin-11* transcriptional regulation in vulval cells.

Immunostaining experiments have indicated that HS is present in vulval cells and around the vulva (Ref. 73 and our unpublished data). Consistent with this finding, abnormal vulval morphogenesis is thought to result from the loss of *rib-2* (a glucosaminyltransferase) function (74). Other glycosyltransferase genes (*sqv-6*, *sqv-2*, *sqv-8*, and *sqv-3*) involved in establishing proteoglycan linkages are required for synthesis of both HS and chondroitin. Mutations of *sqv* genes cause the Sqv phenotype, which was also observed in the *pst-1* mutant. As ample evidence indicates that chondroitin is not sulfated in this organism (34–36), the Sqv phenotype in *pst-1* mutant would be due to undersulfation of HS rather than chondroitin. However, animals with mutations in the *sqv* genes do not exhibit abnormal anterior-posterior cell positioning or small ectopic invaginations (60), despite their requirement for HS synthesis. This apparent discrepancy might be ascribed to the different half-lives of the different gene products studied (mRNA or proteins) and/or to different metabolic functions of the enzymes studied (PAPS transport *versus* GAG linkage). Further study of these genes in the vulval development will provide useful information concerning the fundamental machinery of GAG synthesis and metabolism, as well as the regulation of extracellular signaling by GAGs.

Mutation of *pst-1* also resulted in abnormal EMS cell division and post-embryonic seam cell development, which are regulated by Wnt signaling (75). This gives rise to the intriguing possibility that sulfation of extracellular molecules could be involved in regulation of proteins associated with Wnt signaling in diverse processes in *C. elegans*.

The lethality observed in the *pst-1* mutants isolated in this study occurred at a different embryonic stage than that observed in the *pps-1* null mutant (*tm1109*) that we isolated previously (15). The animals with *pst-1* mutations survived through the embryonic stage of the second generation; in contrast, animals with *pps-1* mutations died in L2/L3 of the first generation. This difference in timing can be explained by several possibilities. (i) Cytosolic sulfation is essential for L2/L3 growth. To date, no null mutation of *ssu-1*, which encodes the only known *C. elegans* ortholog of cytosolic sulfotransferase, has been isolated (76–78). However, deficiencies in *ssu-1*, by RNA interference or reduction-of-function mutations, did not result in a lethal phenotype. (ii) Extracellular sulfation is essential for L2/L3 growth, and PST-1 may not be the only Golgi-resident PAPS transporter, or there may be a novel mechanism for providing PAPS to Golgi-resident sulfotransferases. (iii) Neither cytosolic nor extracellular sulfation is required for L2/L3 growth, and PPS-1 has a function distinct from PAPS synthesis *in vivo*. Understanding how lethality is caused by *pps-1* and *pst-1* deficiencies will shed light on the mechanisms that underlie the regulation of PAPS metabolism and sulfation in *C. elegans* development.

While this manuscript was in preparation, Bülow and colleagues (43) published a paper concentrating on the analysis of *pst-1* and *pst-2* functions in the nervous system of *C. elegans*. They show that *pst-1* is essential in nervous system development and other functions, and our results are complementary to their results indicating the essentiality of PAPS transporters in the organism.

Acknowledgments—We thank Dr. K. Fukushima and Prof. K. Yamashita (Tokyo Institute of Technology, Yokohama, Japan) for providing the mammalian total cDNA. We also thank the Caenorhabditis Genetics Center, which is funded by the National Institutes of Health, NCRR, for the worms and E. coli strains. We also thank Adam Kleinschmit for useful comments.

REFERENCES

1. Kehoe, J. W., and Bertozzi, C. R. (2000) *Chem. Biol.* **7,** R57–R61
2. Schwartz, N. B., and Domowicz, M. (2002) *Glycobiology* **12,** 57R–68R
3. Honke, K., Zhang, Y., Cheng, X., Kotani, N., and Taniguchi, N. (2004) *Glycoconj. J.* **21,** 59–62
4. Zhang, H., Uchimura, K., and Kadomatsu, K. (2006) *Ann. N.Y. Acad. Sci.* **1086,** 81–90
5. Bishop, J. R., Schuksz, M., and Esko, J. D. (2007) *Nature* **446,** 1030–1037
6. Sugahara, K., and Mikami, T. (2007) *Curr. Opin. Struct. Biol.* **17,** 536–545
7. Nadanaka, S., and Kitagawa, H. (2008) *J. Biochem.* **144,** 7–14
8. Morita, I., Kizuka, Y., Kakuda, S., and Oka, S. (2008) *J. Biochem.* **143,** 719–724
9. Robbins, P. W., and Lipmann, F. (1957) *J. Biol. Chem.* **229,** 837–851
10. Klaassen, C. D., and Boles, J. W. (1997) *FASEB J.* **11,** 404–418
11. Strott, C. A. (2002) *Endocr. Rev.* **23,** 703–732
12. Robbins, P. W., and Lipmann, F. (1958) *J. Biol. Chem.* **233,** 681–685
13. Zaruba, M. E., Schwartz, N. B., and Tennekoon, G. I. (1988) *Biochem. Biophys. Res. Commun.* **155,** 1271–1277
14. Besset, S., Vincourt, J. B., Amalric, F., and Girard, J. P. (2000) *FASEB J.* **14,** 345–354
15. Dejima, K., Seko, A., Yamashita, K., Gengyo-Ando, K., Mitani, S., Izumikawa, T., Kitagawa, H., Sugahara, K., Mizuguchi, S., and Nomura, K. (2006) *J. Biol. Chem.* **281,** 11431–11440
16. Schwarz, J. K., Capasso, J. M., and Hirschberg, C. B. (1984) *J. Biol. Chem.* **259,** 3554–3559
17. Carlsson, P., Presto, J., Spillmann, D., Lindahl, U., and Kjellén, L. (2008) *J. Biol. Chem.* **283,** 20008–20014
18. Sohaskey, M. L., Yu, J., Diaz, M. A., Plaas, A. H., and Harland, R. M. (2008) *Development* **135,** 2215–2220
19. Frederick, J. P., Tafari, A. T., Wu, S. M., Megosh, L. C., Chiou, S. T., Irving, R. P., and York, J. D. (2008) *Proc. Natl. Acad. Sci. U.S.A.* **105,** 11605–11612
20. Dick, G., Grøndahl, F., and Prydz, K. (2008) *Glycobiology* **18,** 53–65
21. Capasso, J. M., and Hirschberg, C. B. (1984) *Proc. Natl. Acad. Sci. U.S.A.* **81,** 7051–7055
22. Mandon, E. C., Milla, M. E., Kempner, E., and Hirschberg, C. B. (1994) *Proc. Natl. Acad. Sci. U.S.A.* **91,** 10707–10711
23. Ozeran, J. D., Westley, J., and Schwartz, N. B. (1996) *Biochemistry* **35,** 3695–3703
24. Ozeran, J. D., Westley, J., and Schwartz, N. B. (1996) *Biochemistry* **35,** 3685–3694
25. Kamiyama, S., Suda, T., Ueda, R., Suzuki, M., Okubo, R., Kikuchi, N., Chiba, Y., Goto, S., Toyoda, H., Saigo, K., Watanabe, M., Narimatsu, H., Jigami, Y., and Nishihara, S. (2003) *J. Biol. Chem.* **278,** 25958–25963
26. Kamiyama, S., Sasaki, N., Goda, E., Ui-Tei, K., Saigo, K., Narimatsu, H., Jigami, Y., Kannagi, R., Irimura, T., and Nishihara, S. (2006) *J. Biol. Chem.* **281,** 10945–10953
27. Goda, E., Kamiyama, S., Uno, T., Yoshida, H., Ueyama, M., Kinoshita-Toyoda, A., Toyoda, H., Ueda, R., and Nishihara, S. (2006) *J. Biol. Chem.* **281,** 28508–28517
28. Lüders, F., Segawa, H., Stein, D., Selva, E. M., Perrimon, N., Turco, S. J., and Häcker, U. (2003) *EMBO J.* **22,** 3635–3644
29. Ali, R. A., Mellenthin, K., Fahmy, K., Da Rocha, S., and Baumgartner, S. (2005) *Dev. Genes. Evol.* **215,** 537–543
30. Clément, A., Wiweger, M., von der Hardt, S., Rusch, M. A., Selleck, S. B., Chien, C. B., and Roehl, H. H. (2008) *PLoS Genet.* **4,** e1000136
31. Sherman, T., Chernova, M. N., Clark, J. S., Jiang, L., Alper, S. L., and Nehrke, K. (2005) *Am. J. Physiol. Cell Physiol.* **289,** C341–C351
32. Bülow, H. E., and Hobert, O. (2004) *Neuron* **41,** 723–736
33. Mizuguchi, S., and Dejima, D., and Nomura, K. (2009) *Trends Glycosci. Glycotechnol.* **21,** 179–191
34. Yamada, S., Van Die, I., Van den Eijnden, D. H., Yokota, A., Kitagawa, H., and Sugahara, K. (1999) *FEBS Lett.* **459,** 327–331
35. Toyoda, H., Kinoshita-Toyoda, A., and Selleck, S. B. (2000) *J. Biol. Chem.* **275,** 2269–2275
36. Nabetani, T., Miyazaki, K., Tabuse, Y., and Tsugita, A. (2006) *Proteomics* **6,** 4456–4465
37. Kim, T. H., Hwang, S. B., Jeong, P. Y., Lee, J., and Cho, J. W. (2005) *FEBS Lett.* **579,** 53–58
38. Berninsone, P. M. (December 18, 2006) in *WormBook* (*C. elegans* Research Community, ed) doi/10.1895/wormbook.1.125.1, http://www.wormbook.org
39. Gumienny, T. L., MacNeil, L. T., Wang, H., de Bono, M., Wrana, J. L., and Padgett, R. W. (2007) *Curr. Biol.* **17,** 159–164
40. Franks, D. M., Izumikawa, T., Kitagawa, H., Sugahara, K., and Okkema, P. G. (2006) *Dev. Biol.* **296,** 409–420
41. Kitagawa, H., Izumikawa, T., Mizuguchi, S., Dejima, K., Nomura, K. H., Egusa, N., Taniguchi, F., Tamura, J., Gengyo-Ando, K., Mitani, S., Nomura, K., and Sugahara, K. (2007) *J. Biol. Chem.* **282,** 8533–8544
42. Bülow, H. E., Tjoe, N., Townley, R. A., Didiano, D., van Kuppevelt, T. H., and Hobert, O. (2008) *Curr. Biol.* **18,** 1978–1985
43. Bhattacharya, R., Townley, R. A., Berry, K. L., and Bülow, H. E. (2009) *J. Cell Sci.* **122,** 4492–4504
44. Brenner, S. (1974) *Genetics* **77,** 71–94
45. Burdine, R. D., Branda, C. S., and Stern, M. J. (1998) *Development* **125,** 1083–1093
46. Gupta, B. P., and Sternberg, P. W. (2002) *Dev. Biol.* **247,** 102–115
47. Mohler, W. A., Simske, J. S., Williams-Masson, E. M., Hardin, J. D., and White, J. G. (1998) *Curr. Biol.* **8,** 1087–1090
48. Gengyo-Ando, K., and Mitani, S. (2000) *Biochem. Biophys. Res. Commun.* **269,** 64–69
49. Mizuguchi, S., Uyama, T., Kitagawa, H., Nomura, K. H., Dejima, K., Gengyo-Ando, K., Mitani, S., Sugahara, K., and Nomura, K. (2003) *Nature* **423,** 443–448
50. Izumikawa, T., Kitagawa, H., Mizuguchi, S., Nomura, K. H., Nomura, K., Tamura, J., Gengyo-Ando, K., Mitani, S., and Sugahara, K. (2004) *J. Biol. Chem.* **279,** 53755–53761
51. Kinoshita, A., and Sugahara, K. (1999) *Anal. Biochem.* **269,** 367–378
52. Gravato-Nobre, M. J., Nicholas, H. R., Nijland, R., O'Rourke, D., Whittington, D. E., Yook, K. J., and Hodgkin, J. (2005) *Genetics* **171,** 1033–1045
53. Gengyo-Ando, K., Yoshina, S., Inoue, H., and Mitani, S. (2006) *Biochem. Biophys. Res. Commun.* **349,** 1345–1350
54. Dejima, K., Murata, D., Mizuguchi, S., Nomura, K. H., Gengyo-Ando, K., Mitani, S., Kamiyama, S., Nishihara, S., and Nomura, K. (2009) *FASEB J.* **23,** 2215–2225
55. Gilleard, J. S., Barry, J. D., and Johnstone, I. L. (1997) *Mol. Cell. Biol.* **17,** 2301–2311
56. Mello, C., and Fire, A. (1995) *Methods Cell Biol.* **48,** 451–482
57. Miller, D. M., and Shakes, D. C. (1995) *Methods Cell Biol.* **48,** 365–394
58. Käll, L., Krogh, A., and Sonnhammer, E. L. (2005) *Bioinformatics* **21,** Suppl. 1, i251–i257
59. Käll, L., Krogh, A., and Sonnhammer, E. L. (2007) *Nucleic Acids Res.* **35,** W429-W432
60. Herman, T., Hartwieg, E., and Horvitz, H. R. (1999) *Proc. Natl. Acad. Sci. U.S.A.* **96,** 968–973
61. Hwang, H. Y., Olson, S. K., Esko, J. D., and Horvitz, H. R. (2003) *Nature* **423,** 439–443
62. Morio, H., Honda, Y., Toyoda, H., Nakajima, M., Kurosawa, H., and Shirasawa, T. (2003) *Biochem. Biophys. Res. Commun.* **301,** 317–323
63. Chisholm, A. D., and Hardin, J. (December 01, 2005) in *WormBook* (*C. elegans* Research Community, ed) doi/10.1895/wormbook.1.35.1, http://www.wormbook.org
64. Wang, X., Zhao, Y., Wong, K., Ehlers, P., Kohara, Y., Jones, S. J., Marra, M. A., Holt, R. A., Moerman, D. G., and Hansen, D. (2009) *BMC Genomics* **10,** 213
65. Yano, H., Yamamoto-Hino, M., Abe, M., Kuwahara, R., Haraguchi, S., Kusaka, I., Awano, W., Kinoshita-Toyoda, A., Toyoda, H., and Goto, S. (2005) *Proc. Natl. Acad. Sci. U.S.A.* **102,** 13467–13472
66. Silbert, J. E., and Sugumaran, G. (1995) *Biochim. Biophys. Acta* **1241,** 371–384
67. Nelson, F. K., Albert, P. S., and Riddle, D. L. (1983) *J. Ultrastruct. Res.* **82,** 156–171
68. Höflich, J., Berninsone, P., Göbel, C., Gravato-Nobre, M. J., Libby, B. J., Darby, C., Politz, S. M., Hodgkin, J., Hirschberg, C. B., and Baumeister, R. (2004) *J. Biol. Chem.* **279,** 30440–30448

69. Cipollo, J. F., Awad, A. M., Costello, C. E., and Hirschberg, C. B. (2004) *J. Biol. Chem.* **279,** 52893–52903
70. Sternberg, P. W., and Horvitz, H. R. (1988) *Dev. Biol.* **130,** 67–73
71. Sawa, H., Lobel, L., and Horvitz, H. R. (1996) *Genes Dev.* **10,** 2189–2197
72. Lin, X. (2004) *Development* **131,** 6009–6021
73. Minniti, A. N., Labarca, M., Hurtado, C., and Brandan, E. (2004) *J. Cell Sci.* **117,** 5179–5190
74. Bender, A. M., Kirienko, N. V., Olson, S. K., Esko, J. D., and Fay, D. S. (2007) *Dev. Biol.* **302,** 448–462
75. Eisenmann, D. M. (June 25, 2005) in *WormBook* (*C. elegans* Research Community, ed) doi/10.1895/wormbook.1.7.1, http://www.wormbook.org
76. Carroll, B. T., Dubyak, G. R., Sedensky, M. M., and Morgan, P. G. (2006) *J. Biol. Chem.* **281,** 35989–35996
77. Hattori, K., Inoue, M., Inoue, T., Arai, H., and Tamura, H. O. (2006) *J. Biochem.* **139,** 355–362
78. Sönnichsen, B., Koski, L. B., Walsh, A., Marschall, P., Neumann, B., Brehm, M., Alleaume, A. M., Artelt, J., Bettencourt, P., Cassin, E., Hewitson, M., Holz, C., Khan, M., Lazik, S., Martin, C., Nitzsche, B., Ruer, M., Stamford, J., Winzi, M., Heinkel, R., Röder, M., Finell, J., Häntsch, H., Jones, S. J., Jones, M., Piano, F., Gunsalus, K. C., Oegema, K., Gönczy, P., Coulson, A., Hyman, A. A., and Echeverri, C. J. (2005) *Nature* **434,** 462–469